ORIGINAL ARTICLE

Experimental study on longitudinal-torsional ultrasonic vibration drilling of carbon fiber–reinforced plastics/titanium alloy stacks

Zhiyuan Zhou[1] · Yong Feng[1,2] · Weiwei Xu[1] · Haojie Zhou[1] · Yuyan Qin[1] · Xiaolin Jia[1]

Abstract

Carbon fiber–reinforced plastics (CFRP)/titanium alloy (Ti) stacks are extensively applied in the aerospace industry due to their excellent mechanical properties. However, their poor machinability poses great challenges. In this study, longitudinal-torsional ultrasonic vibration drilling (LT-UVD) is innovatively introduced to improve the quality of CFRP/Ti drilling. First, the separation mode of LT-UVD is analyzed by kinematic equations. Then, an experimental platform is built based on the LT-UVD vibration actuator to perform CFRP/Ti drilling experiments. The thrust force, interface temperature, hole wall quality, hole defects, Ti chip morphologies, and tool wear in LT-UVD are experimentally compared against conventional drilling (CD) and longitudinal ultrasonic vibration drilling (L-UVD). The experimental results show that, compared with CD and L-UVD, the thrust force of CFRP in LT-UVD decreases by 20.36–40.55% and 2.04–14.61%, while the thrust force of Ti decreases by 19.08–24.83% and 1.95–9.34%. Moreover, a relatively low maximum interface temperature is achieved in LT-UVD. In addition, the hole size accuracy, surface roughness for the hole's inner surface, and delamination factor are improved in LT-UVD. Fiber pullout defects, chip-breaking performance, and tool wear of CFRP are improved due to torsional vibration in LT-UVD. Finally, according to the high-speed camera, damage forms of the interface area are different when drilling CFRP/Ti stacks with various drilling sequences.

Keywords CFRP/Ti stacks · Ultrasonic drilling · LT-UVD · Defect suppression · Surface integrity

1 Introduction

Carbon fiber–reinforced plastics (CFRP) and titanium alloy (Ti) are widely used in aerospace applications due to their lightweight, good corrosion and fatigue resistance, and high specific modulus and intensity [1, 2]. To fully utilize the excellent properties of CFRP and Ti in aerospace applications, the two materials are usually superimposed to form CFRP/Ti stacks [3]. CFRP/Ti stacks are usually riveted or bolted in aircraft assembly, which requires many high-precision connection holes [4, 5]. Mechanical drilling of CFRP/Ti stacks is one of the most extensively hole-making methods in the aviation manufacturing industry [6].

One-shot drilling of CFRP/Ti stacks remains the mainstream technology for manufacturing holes. However, the machining properties of CFRP and Ti are quite different, resulting in difficult hole machining [7]. A decrease in hole wall accuracy and quality caused by machining seriously affects the fatigue performance and strength of aircraft structural parts [8]. Therefore, reducing the processing damage of the connecting hole and improving the bearing strength and fatigue life of CFRP/Ti stacks are still research hotspots and urgent problems that need to be solved.

Some researchers have conducted conventional drilling (CD) experiments, trying to improve the drilling damage defects of CFRP/Ti stacks by selecting different process parameters and different bit geometries. They found that high spindle speed and low feed rate can effectively minimize drilling-induced defects, suppress the wear of drill bits, and reduce delamination defects and interface layer damage [9, 10]. In addition, changing the drill bit geometry or bit type can effectively improve the drilling stability and chip-breaking performance and reduce the delamination defects [11–14]. CD is a common drilling method with

✉ Yong Feng
  fengyong007@sina.com

[1] School of Mechanical Engineering, Nanjing Institute of Technology, Nanjing 211167, Jiangsu, China

[2] School of Mechanical Engineering, Changshu Institute of Technology, Suzhou 215506, Jiangsu, China

high production efficiency and low cost. However, with the continuous improvement of the precision requirements of CFRP/Ti stacks in the aircraft manufacturing industry, it is not easy to meet high-precision drilling requirements with small hole quality improvement by choosing reasonable drill bit geometries and process parameters in CD.

Longitudinal ultrasonic vibration drilling (L-UVD) is a non-traditional hybrid process widely used in CFRP/Ti stack hole making. L-UVD solved the problems of excessive drilling thrust force in CD and improved the quality of the processed hole wall. Shao et al. [15] innovatively applied L-UVD to CFRP/Ti stack drilling. The experimental results indicated that the thrust force of CFRP and Ti in L-UVD decreased by 41.2–46.8% and 15.2–26.1% compared with CD, respectively. Moreover, Shao et al. [16] focused on the interface temperature of CFRP/Ti stacks in L-UVD. The experimental results showed that the duration of exceeding the CFRP glass transition temperature and the maximum interface temperature was reduced by approximately 52.2% and 22.8% compared to CD, respectively. It was proven that ultrasonic vibration drilling could effectively reduce the drilling temperature. Dahnel et al. [17] considered using L-UVD in drilling CFRP/Ti stacks to improve hole quality and tool life. The experimental results showed that, compared with CD, L-UVD reduced the tool wear, including titanium adhesion, abrasive wear, and major edge chipping associated with the drilling of CFRP/Ti stacks. The above studies showed that L-UVD could effectively reduce interface temperature, drilling thrust force, and tool wear.

However, one-dimensional vibration only changes the longitudinal separation effect between the tool and the workpiece, while the contact in the torsional direction is not effectively improved. There are still many problems, such as delamination and fiber pullout [18]. Recently, many researchers have found that 2D longitudinal-torsional ultrasonic vibration drilling (LT-UVD) has great potential application for drilling CFRP and Ti. Ma et al. [19] drilled CFRP with LT-UVD. The experimental results indicated that LT-UVD reduced the thrust force by 39% and effectively suppressed CFRP delamination and burr defects compared with CD. Wang et al. [20] analyzed the feasibility of LT-UVD on CFRP by observing the drilling dynamics and motion properties of LT-UVD. The results showed that LT-UVD improved the hole wall quality of CFRP and reduced delamination defects. Liu et al. [21] found that, compared with CD, the LT-UVD thrust force was reduced by 30%, and the delamination factor was reduced by 69.67% in CFRP drilling. Moreover, Tian et al. [22] conducted LT-UVD experiments on Ti6Al4V. The authors observed that the tool wear was reduced compared to L-UVD. Gao et al. [23] investigated the effect of LT-UVD on Ti6Al4V micro-holes. Compared with CD, the morphology of chips in LT-UVD presented as smaller and

more fragmentary, the thrust force was correspondingly reduced by 1.98–24.9%, and burr defect was effectively suppressed, which demonstrated the effectiveness of drilling Ti6Al4V with LT-UVD.

Most of the existing research on LT-UVD focuses on drilling an individual CFRP or Ti, and there are few reports on the drilling of CFRP/Ti stacks. In this study, a self-built LT-UVD device is used to perform drilling experiments on CFRP/Ti stacks, and the results are compared with L-UVD and CD. The thrust force, interface layer temperature, hole wall quality, and hole defects are comprehensively analyzed. The results obtained in this paper will help reduce the hole damage defects of CFRP/Ti stacks and provide reliable reference for drilling high-precision and low-damage CFRP/Ti stacks in aviation manufacturing.

2 Analysis of LT-UVD motion characteristics

Figure 1 shows the process of machining CFRP/Ti stacks with LT-UVD. Due to the unique structure of CFRP/Ti stacks, there are multiple states of tool-material interaction, which makes the drilling process extremely unstable. Longitudinal and torsional ultrasonic vibrations are added to the tool to form a more complex 2D ultrasonic vibration, improve the drilling quality, and increase the drilling stability. The vibration form is shown in Fig. 1. Periodic high-frequency longitudinal-torsional vibration of the tool changes the tool trajectory and the cutting mechanism.

It is necessary to analyze the motion trail of the cutter to clarify the cutting mechanism of LT-UVD and enhance processing reliability. Assuming that point O is located on the drill bit at a radius of r, point O is r' away from the axis in the radial direction. Furthermore, the turning angle of point O with time is $\theta = 2\pi n t$. Based on the related positions of the cutter and the workpiece shown in Fig. 1, θ should be a negative value. The motion trail of point O in the conventional drilling (CD) can be described as follows:

$$\begin{cases} x_c = r'\cos(2\pi n t) = r'\cos(\theta) \\ y_c = r'\sin(2\pi n t) = r'\sin(\theta) \\ z_c = V_f n t = V_f \theta/(2\pi) \end{cases} \quad (1)$$

where n denotes the rotating speed of the spindle and V_f denotes the axial feed speed. Longitudinal ultrasonic vibration drilling (L-UVD) adds longitudinal ultrasonic vibration based on CD. The longitudinal motion trail of L-UVD can be obtained by superimposing the vibration-induced periodic displacement onto the axial feed displacement, as shown in Eq. (2). The longitudinal displacement of L-UVD can be written as:
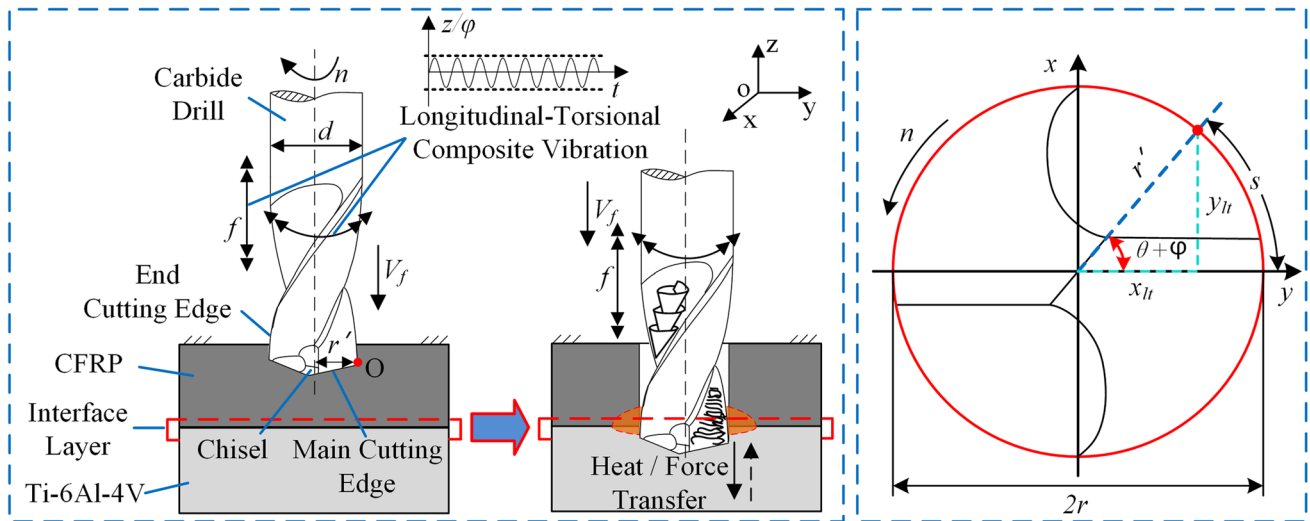
Fig. 1 Illustration of the LT-UVD process

$$z_l = \frac{V_f \theta}{2\pi} + A\sin(f\theta/n) \qquad (2)$$

where A denotes the ultrasonic axial vibration amplitude, and f denotes the ultrasonic vibration frequency. The vibration of the cutter in LT-UVD is composed of longitudinal and torsional vibration. The longitudinal motion is identical to the L-UVD motion, while the torsional motion adds the torsional vibration based on the original drilling rotation. The additional rotation angle φ induced by torsional vibration obeys the following time dependence:

$$\varphi = A_\varphi \sin(f\theta/n) \qquad (3)$$

where A_φ denotes the amplitude of torsional vibration. By combining Eqs. (2) and (3), the motion trail of LT-UVD can be expressed as follows:

$$\begin{cases} x_{lt} = r'\cos(\theta + \varphi) \\ y_{lt} = r'\sin(\theta + \varphi) \\ z_{lt} = \frac{V_f \theta}{2\pi} + A\sin(f\theta/n) \end{cases} \qquad (4)$$

Figure 2 displays the 3D motion trails of point O at the edge using CD, L-UVD, and LT-UVD. The process parameters are $r' = 3$ mm, $n = 1800$ rev/min, $V_f = 10$ mm/min, $A = 2.5$ μm, $A_\varphi = 1.65$ μm, and $f = 35$ kHz. The motion curve of CD is a smooth helical curve, the motion curve of L-UVD consists of the helical curve and sinusoidal curve, and the motion curve of LT-UVD consists of a helical curve and the sinusoidal curve at a certain inclination angle.

The 3D motion trail of a point on the cutter can be expanded and transformed into a more visual 2D motion to further explore the difference between the three cutting modes. In the 2D motion, the motion trail of LT-UVD can
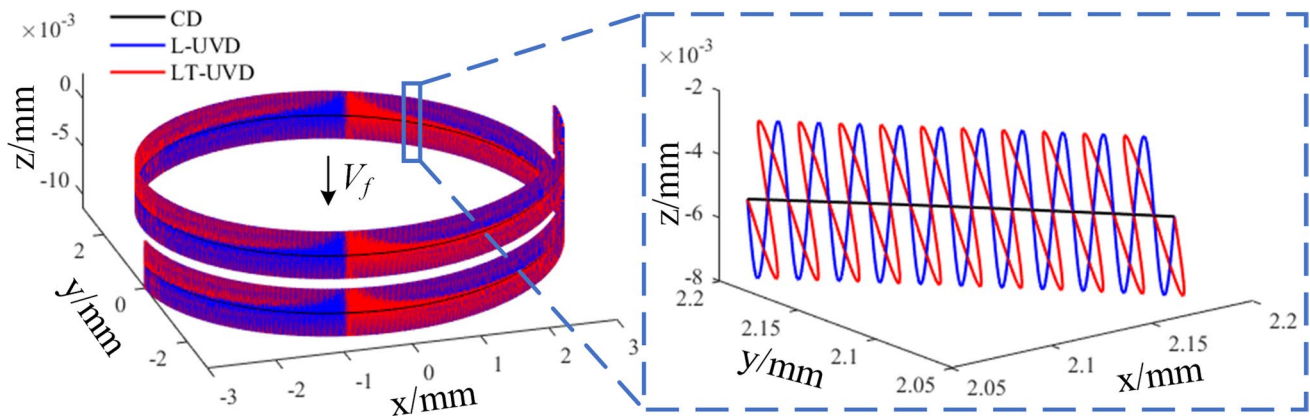

Fig. 2 3D motion trails of point O in CD, L-UVD, and LT-UVD

be decomposed into the superimposition of longitudinal and torsional displacement. According to the definition of the 2D tool coordinate system in Fig. 1, the torsional displacement of the tool can be obtained as $s = r'(\theta + \varphi)$. The motion equation can then be described as follows:

$$\begin{cases} s = r'(\theta + A_\varphi \sin(f\theta/n)) \\ z = \frac{V_f\theta}{2\pi} + A\sin(f\theta/n) \end{cases} \quad (5)$$

where z denotes the longitudinal displacement. The 2D motion trails using three drilling modes can be drawn according to Eq. (5), as shown in Fig. 3. The process parameters are $r' = 3$ mm, $n = 1800$ rev/min, $V_f = 10$ mm/min, $A = 2.5$ μm, $A_\varphi = 1.65$ μm, and $f = 35$ kHz. Identical to 3D motion curves, the 2D motion curve of CD (marked in black) is a straight line. The 2D motion curve of L-UVD (marked in blue) is sinusoidal due to the periodic vibration in the longitudinal direction. For both machining methods, the tool always cuts the workpiece forward with feed. However, according to the 2D motion trail of LT-UVD (marked in red), the motion trail changes due to unique torsional vibration in LT-UVD. Accordingly, the cutter in LT-UVD moves backward, as marked by the red dashed line in Fig. 3. The cutter shows no forward workpiece cutting at this phase. Accordingly, the cutter can only cut materials upwards. Moreover, the fibers are easily cut off along the cutting direction. The cutting characteristics can reduce thrust force and cutting temperature while effectively inhibiting the wear of the cutter.

3 Experimental research design

3.1 Establishment of experimental devices and the test system

The experiment was performed in a 5-axis processing center (VMC C3OH, Shanghai TOP Numerical Control
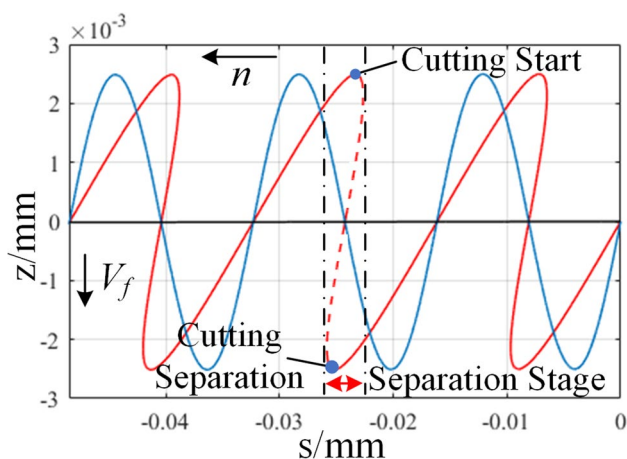

Fig. 3 2D motion trails of point O in CD, L-UVD, and LT-UVD

Technology Co., Ltd., China). As shown in Figs. 4 and 5, the experimental platform mainly consists of the ultrasonic vibration drilling device, the temperature-measuring system, the force-measuring system, and the high-speed camera image acquisition device.

Specifically, the SZ-12 ultrasonic vibration drilling device comprises an ultrasonic power supply, a wireless signal transmission system, and two ultrasonic vibration actuators. The ultrasonic power supply converts the commercial power at a frequency of 50 Hz into a high-frequency alternate-current (AC) electric signal. Then, the AC signal is transmitted to the piezoelectric transducer via the wireless transmission system to generate vibration. Different structures of vibration actuators are important factors that generate longitudinal and torsional vibration, as shown in Fig. 4. The unique spiral groove structure applied to the vibration actuators is the key to generating longitudinal-torsional ultrasonic vibration. During the experiment, the longitudinal-to-torsional amplitude conversion ratio was 0.66 [20], while the longitudinal and the torsional amplitudes were 2.5 μm and 1.65 μm, respectively.

The force-measuring system mainly comprises piezoelectric four-component force meters (9272, Kistler, Switzerland). The force measurement data were collected and amplified by the charge amplifier (5080A, Kistler, Switzerland), and finally transmitted to the software on the PC (DynoWare) for signal analysis and drilling force processing.

The multi-channel signal analyzer (DH5922N, Donghua Test, China) was used to acquire the electric signal and transmit it to MFC AppWizard software on a PC for temperature monitoring. The acquisition frequency was set to 1 kHz. Electrical signals are collected by sheet K-type thermocouples connected to the multi-channel signal analyzer. The thermocouple covers a wide temperature measurement range from -20 to 500 ℃.

The drilling process of laminated materials was recorded with a high-speed camera in this paper due to unclear drilling mechanisms and complex thermodynamic action in the transitional region at the laminated material interface. Accordingly, the drilling-caused damage process and surface integrity in the interface transitional region can be investigated in depth. The high-speed camera system is mainly composed of a high-resolution particle imaging velocimeter (HiSense Zyla 5.5 MP sCMOS, Dantec Dynamics, Denmark) and micro-lens (atx-i 100 mm F2.8 FF MACRO, Tokina, Japan), as shown in Fig. 5. The camera system is connected to the image acquisition software on PC (Dynamic Studio7.6, Dantec Dynamics, Denmark) to achieve a frame-by-frame detailed record of the drilling process of laminated materials. During shooting, the high-speed camera lens is parallel to the upper surface
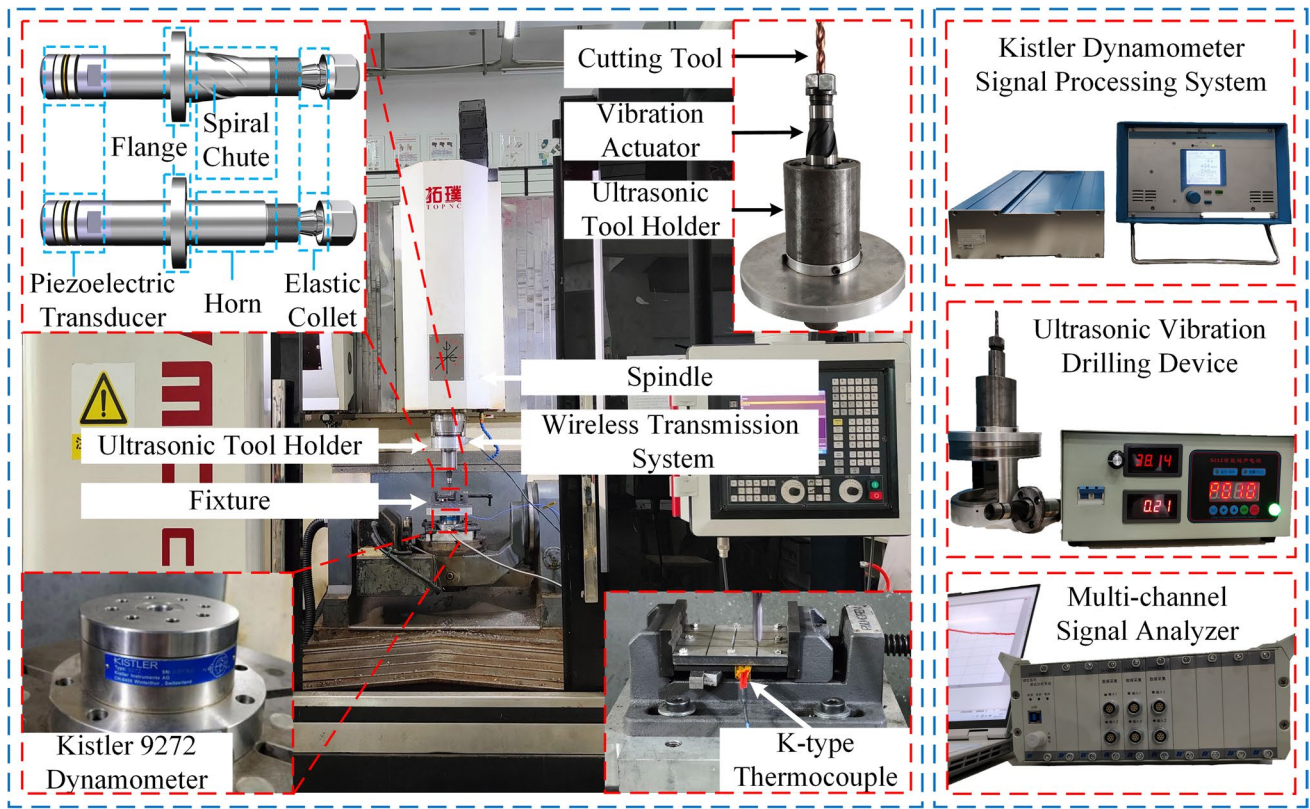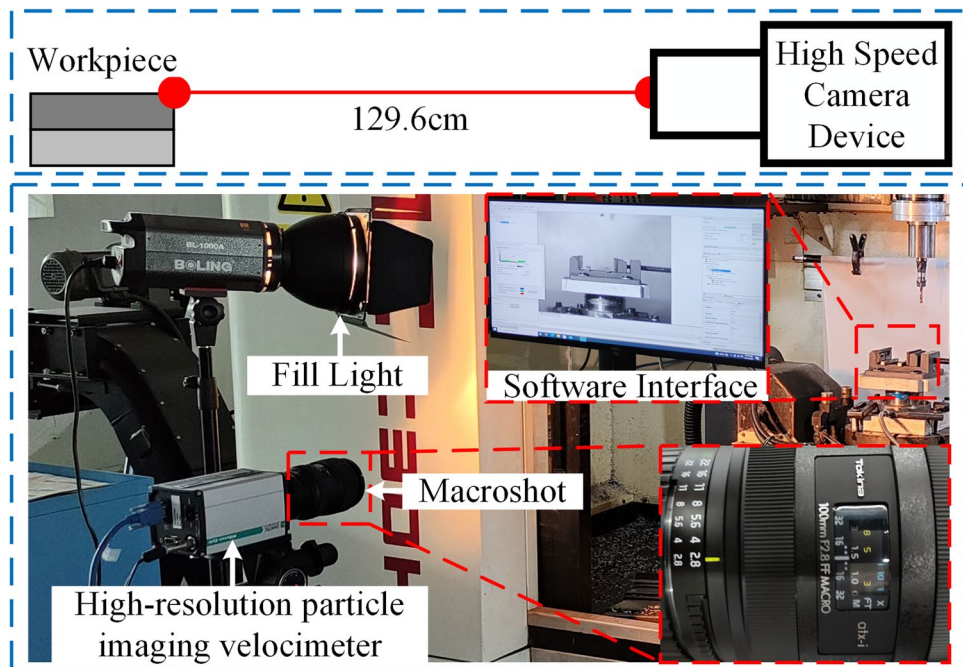
Fig. 4 Experimental platform and measurement programs

Fig. 5 High-speed camera experiment

of the workpiece at a distance of 129.6 cm. Lens focusing settings and aperture parameters are shown in Fig. 5.

3.2 Materials and cutter

In this study, the workpiece comprises a CFRP plate and a Ti plate. CFRP plates were manufactured by Chengdu Aircraft Industry Group Co., Ltd., with a length × width × thickness of 75 mm × 75 mm × 4.7 mm. CFRP is made up of carbon fibers and epoxy resin. The upper and lower surfaces of CFRP plates are made of carbon fiber plain-weave fabrics and an anti-electromagnetic interference fibrous layer. As shown in Fig. 6a, the upper and the lower surfaces are 0.1 mm and 0.6 mm in thickness, with the fiber direction of 0/90°. The middle part of CFRP is a unidirectional fiber ply with a direction of $[0°/-45°/45°/90°]_S$. The thickness of a single carbon fiber ply layer is 0.25 mm, and 16 layers are employed, i.e., the total thickness is 4 mm. For the CFRP plates, the tensile strength is 1200 MPa, and Young's modulus is 145 GPa. The employed titanium alloy was Ti6Al4V, with the same length and width dimensions as CFRP and a thickness of 6 mm. The hardness of the Ti plate is 41 HRC, the yield strength is 880 MPa, and Young's modulus is 114 GPa. During the experiment, the carbon fiber plates and Ti plates were fastened by the bolted connection mode commonly used for aircraft CFRP/Ti components to avoid the effect of the adhesive method on the interface layer during drilling.

Two types of cutters were used, as shown in Fig. 6b and c. The uncoated hard-alloy drilling bit (860.1–0640-020A1-SM 1210, SANDVIK) with a diameter of 6.4 mm was used during the vibration drilling experiment. When using the high-speed camera for shooting, the PVD TiAlN–coated drilling bit (R846-0800–30-A1A 1220, SANDVIK) with a diameter of 8 mm was used for additional visual display.

3.3 Experimental design

During the dry-cutting experiment [15, 24], the CFRP/Ti stacks were drilled with CD, L-UVD, and LT-UVD to examine the cutting speed and vibration mode effects on drilling quality. Moreover, considering the feasibility of two drilling sequences (from the CFRP plate and the Ti plate, denoted as C to T and T to C, respectively) [25, 26]. The experiments also compared the performances using two different drilling sequences. A new cutter was used in each experimental group to avoid cutter wear on the obtained experimental results. Table 1 lists the detailed experimental parameters.

4 Experimental results and discussion

4.1 Thrust force

Figure 7 shows a typical thrust force curve of LT-UVD for different drilling sequences (C to T and T to C), during which the cutting parameters were the same ($n = 10$ mm/min and $V_f = 1200$ r/min). Regardless of the drilling direction (from C to T or from T to C), CFRP/Ti stacks show

Fig. 6 **a** CFRP/Ti workpiece, **b** uncoated hard-alloy drilling bit (Φ6.4 mm), and **c** PVD TiAlN–coated drilling bit (Φ8 mm)
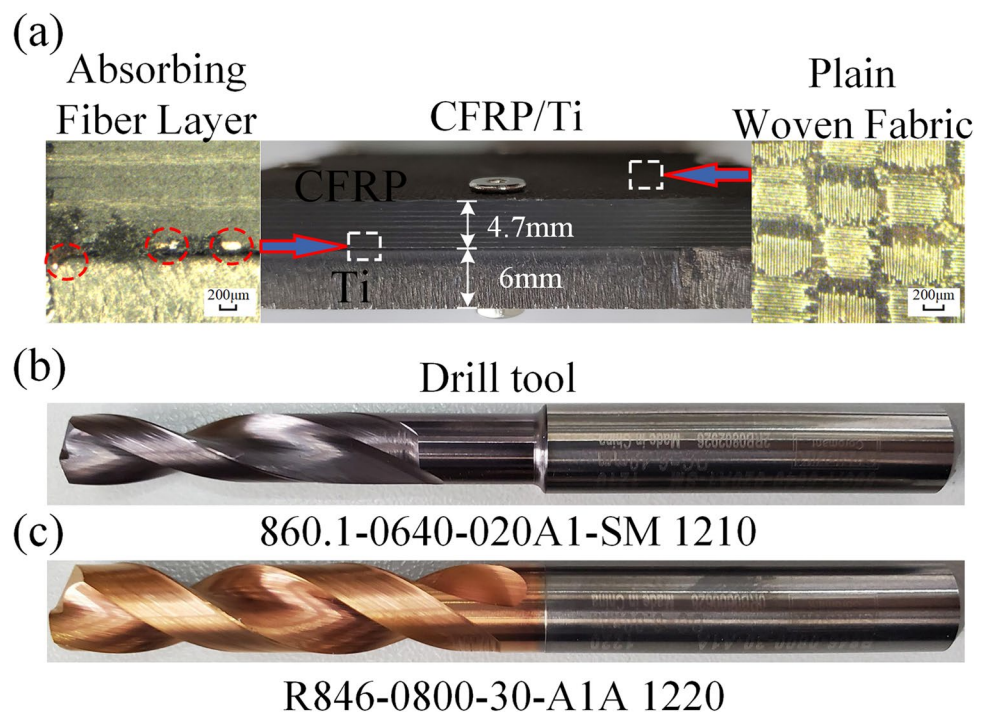
Table 1 Experimental conditions

	Process parameters					
	Spindle speed n (rev/min)	Feed speed V_f (mm/min)	Frequency f (kHz)	Longitudinal amplitude A (μm)	Torsional amplitude A_φ (μm)	Stacking direction
CD	1200	10	0	0	0	C to T, T to C
L-UVD	1200, 1500, 1800	10	35	2.5	0	C to T, T to C
LT-UAD	1200, 1500, 1800	10	35	2.5	1.65	C to T, T to C
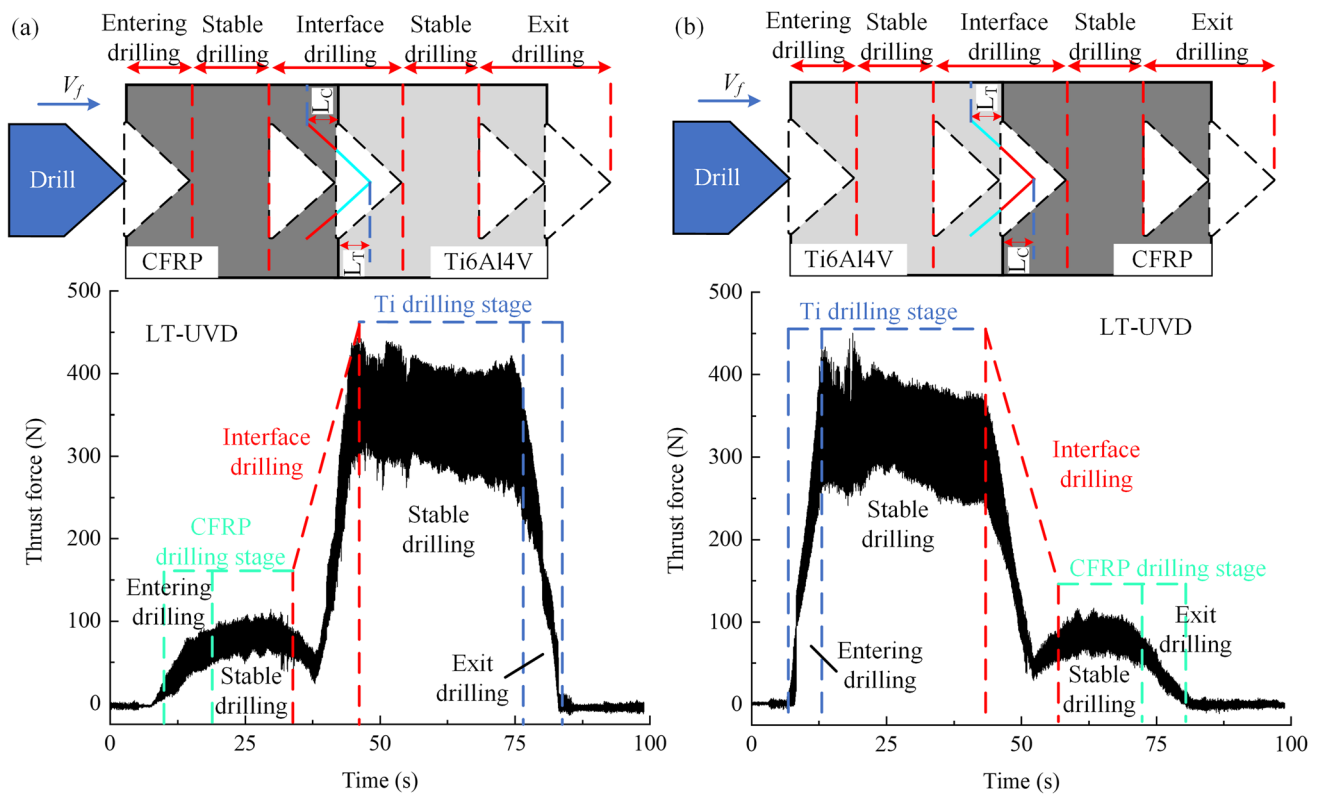
Fig. 7 Typical thrust force curve of LT-UVD for different drilling sequences (**a** C to T and **b** T to C) when $n = 10$ mm/min and $V_f = 1200$ r/min, and illustration of the CFRP/Ti drilling phase

identical shapes after drilling. The drilling process can be divided into five phases:

(i) When the chisel edge of the cutter contacts the material, the thrust force rapidly increases in a short time due to the interaction between the cutter and the material.

(ii) When the drill tip fully enters, the drilling process remains stable. At that moment, the thrust force remains approximately stable.

(iii) As the tool is continuously fed, it starts cutting the interface area. Figure 7 shows the interface drilling process under different stacking sequences, in which

L_C and L_T represent the components of the main cutting edge in cutting CFRP and Ti, respectively. When L_C and L_T are not equal to 0, the cutter is located in the interface region and simultaneously drills CFRP and Ti under a coupled interaction.

(iv) Once the drilling tip fully penetrated the interface layer, the drilling entered a stable phase, and the thermal force varied stably.

(v) Finally, the drilling phase was finished. The drilling tip is drilled out of the workpiece until the process is completed.

Figure 8 compares the thrust forces generated by CFRP/Ti using three different technologies with different drilling sequences and the same drilling parameters ($n = 10$ mm/min and $V_f = 1200$ r/min). The thrust forces generated in L-UVD and LT-UVD with ultrasonic vibration dropped significantly. Compared with the CD results, the thrust forces generated by CFRP drilling using L-UVD dropped by 31.54% and 16.27% when drilling from C to T and T to C, respectively. On the other hand, the thrust forces generated by the drilling of Ti dropped by 22.97% and 17.37% when drilling from C to T

and T to C, respectively. Using LT-UVD, the thrust forces generated by CFRP were reduced by 40.55% and 20.36% when drilling from C to T and T to C. Lastly, the thrust forces generated by Ti drilling were reduced by 24.83% and 19.80% when drilling from C to T and T to C.

Moreover, for the drilling sequence from T to C, the thrust force was generally lower than the thrust force when drilling from C to T, which can be attributed to the chip removal of Ti. Ti chips passed through CFRP-machined hole walls when removed in the C to T drilling sequence. The chip removal distance was prolonged, which can easily cause the blockage of chips, accelerate the friction between chips and the hole wall, and increase the thrust force.

Figure 9 shows the thrust forces generated during the processing of CFRP/Ti with L-UVD and LT-UVD at different rotating speeds. As shown in Fig. 9a, when drilling from C to T, the thrust forces generated by the drilling of CFRP and Ti with LT-UVD were reduced by 2.04–13.16% and 1.95–4.02% compared with the values with L-UVD, respectively. As shown in Fig. 9b, when drilling from T to C, the thrust forces generated by the drilling of CFRP and Ti with LT-UVD were reduced by 4.89–14.61% and 2.07–9.34% compared with the values with L-UVD, respectively. Thus, it can be concluded that the thrust forces can be significantly reduced via LT-UVD during CFRP/Ti processing. This is because unique torsional vibration in LT-UVD changed the cutting and separation modes between the cutter and the workpiece. Periodic high-frequency longitudinal-torsional vibration enhanced the cutting performance of the drilling cutter, improved the chip-breaking effect, and reduced friction. In addition, it can also be observed that the thrust
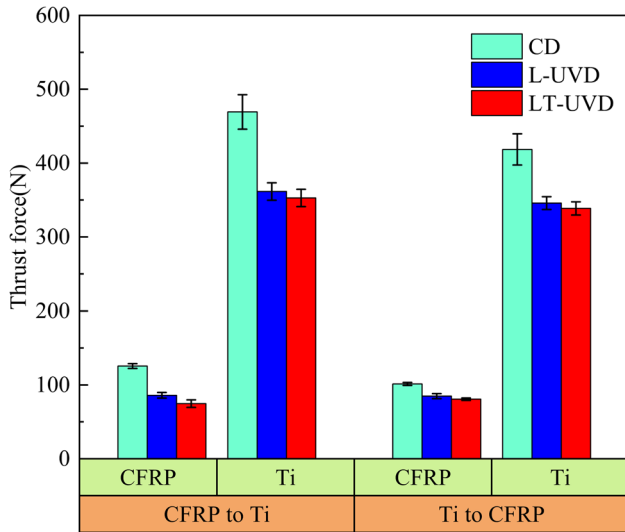

Fig. 8 Thrust forces using CD, L-UVD, and LT-UVD when $n = 10$ mm/min and $V_f = 1200$ r/min
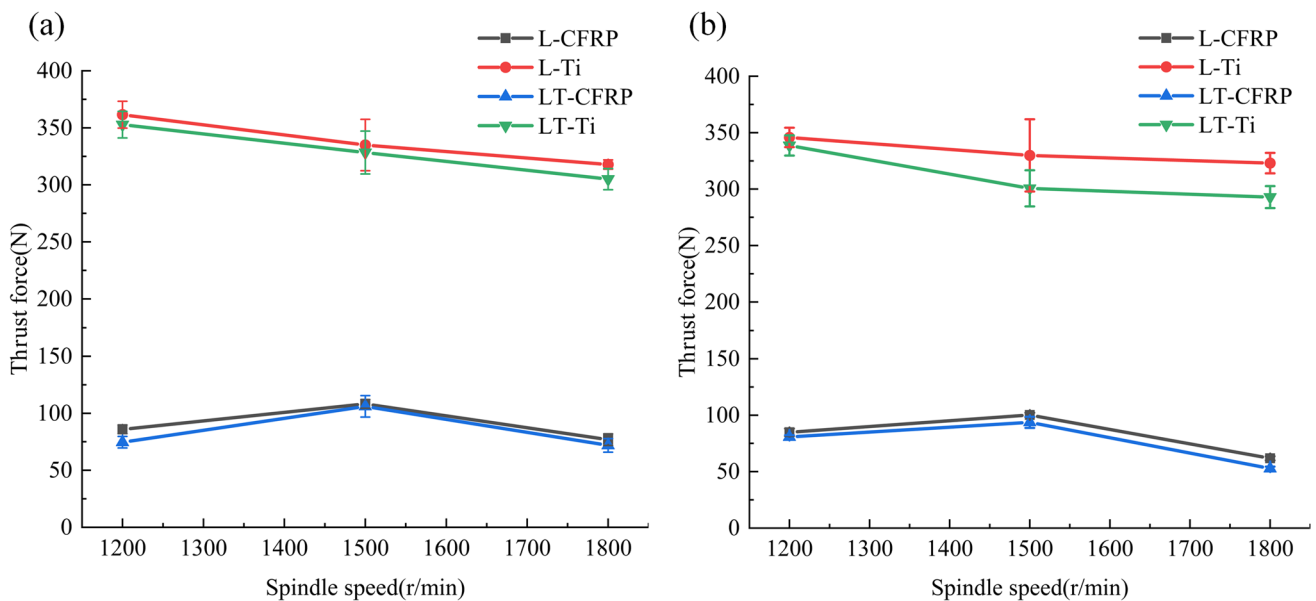

Fig. 9 Thrust forces on CRFP and Ti using L-UVD and LT-UVD at different rotating speeds: **a** C to T and **b** T to C

force dropped with an increase in the rotating speed during Ti drilling, while the thrust force first increased and then dropped during CFRP drilling. This indicates that the high rotating speed can reduce the thrust force when drilling CFRP/Ti stacks.

4.2 Interface temperature

During the drilling of CFRP/Ti stacks, the heat accumulated at the interface is the main reason that causes heat injuries at the interface. These injuries may seriously lower the fatigue strength of materials and affect the service life [16]. Therefore, sheet thermocouples were employed in this study to record the temperature changes at the interface and analyze them in depth based on the measured maximum interface temperature.

Figure 10 shows the installation method of K-type thermocouples. The thickness of the thermocouple end sheet is 0.15 mm. Because of the small thickness of the sheet, it will not affect the drilling after the stacking material is clamped. The sheet was held on the interface layer at a distance of 0.2 mm from the edge of the drilled hole. Therefore, the temperature of the interface layer during the drilling process can be effectively measured, and the temperature measurement groove can be avoided in advance to ensure the accuracy of the data in drilling.

Figure 11a and b show temperature variation curves at the interface using CD, L-UVD, and LT-UVD for the same processing parameters ($n = 10$ mm/min and $V_f = 1200$ r/min). It can be observed that the maximum temperatures at the interface using different drilling sequences show similar variation rules. The temperatures during L-UVD and LT-UVD ultrasonic vibration drilling were far significantly lower than

during CD drilling. As shown in Fig. 11a, the maximum interface temperatures with L-UVD and LT-UVD dropped by 30.29% and 35.23%, respectively, compared to CD values. As shown in Fig. 11b, the maximum interface temperatures with L-UVD and LT-UVD were 32.84% and 39.05% lower than the CD value, respectively. In combination with actual temperature curves, the temperature at the interface was mainly sourced from Ti. The above measurement results show that L-UVD and LT-UVD further reduced the friction between the cutter and the workpiece during Ti processing and enhanced the drilling performance.

Figure 12 shows the maximum temperatures at the CFRP/Ti interface with L-UVD and LT-UVD for different rotating speeds of main shafts, during which two different drilling sequences were used. When drilling from C to T, the maximum temperature using LT-UVD dropped by 7.09–7.98% compared to the value when L-UVD was employed. When drilling from T to C, the maximum temperature using LT-UVD was reduced by 6.11–12.36%. A decline in the maximum temperature can be attributed to the improvement of chip removal and friction performance during processing. When L-UVD and LT-UVD were employed, the maximum temperature from T to C was slightly lower than from C to T. According to Fig. 12, the maximum interface temperature increased with the rotating speed of the main shaft in L-UVD and LT-UVD.

4.3 Hole quality analysis

Hole quality is the key to ensuring aircraft components' safe and stable operation while drilling CFRP/Ti stacks. Dimensional precision of the bolt connection hole, surface roughness, delamination defects of composite materials, fiber pullout, and
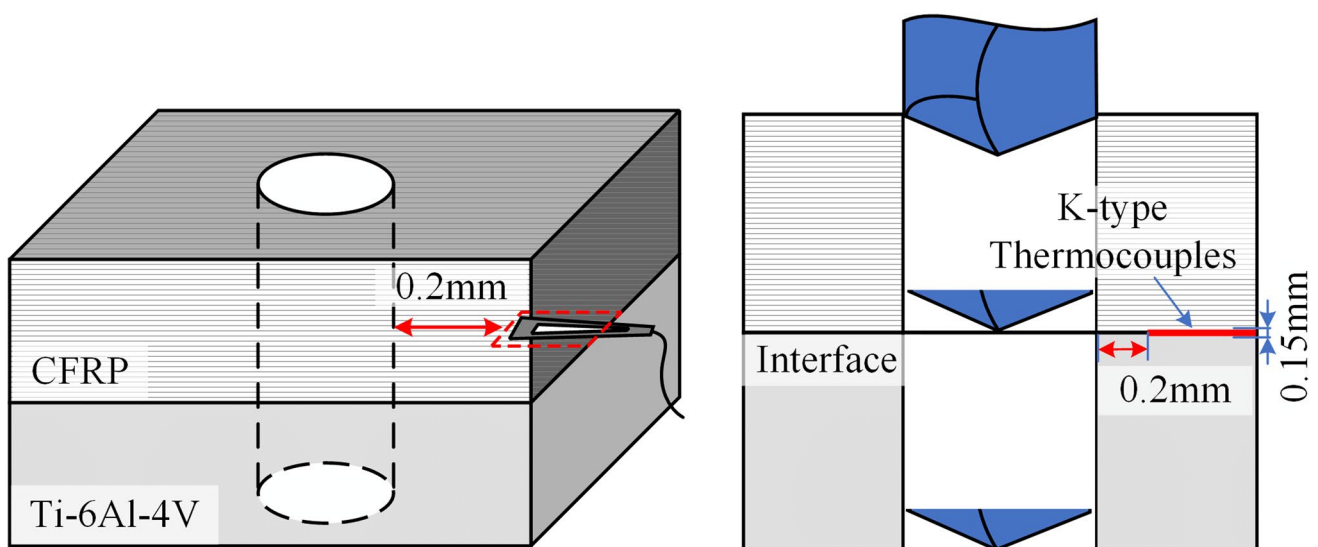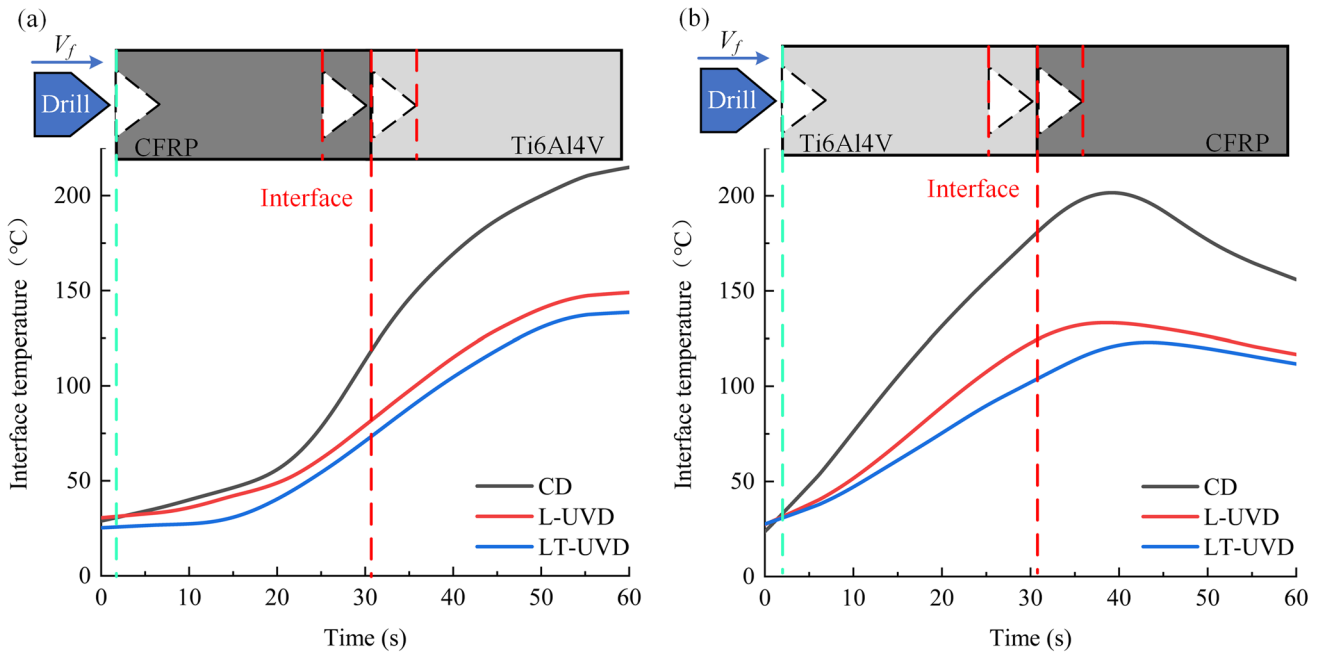

Fig. 10 The interface temperature measurement

Fig. 11 Curves of interfacial temperature of LT-UVD under different drilling sequences for the same processing parameters $n = 10$ mm/min and $V_f = 1200$ r/min: **a** C to T and **b** T to C
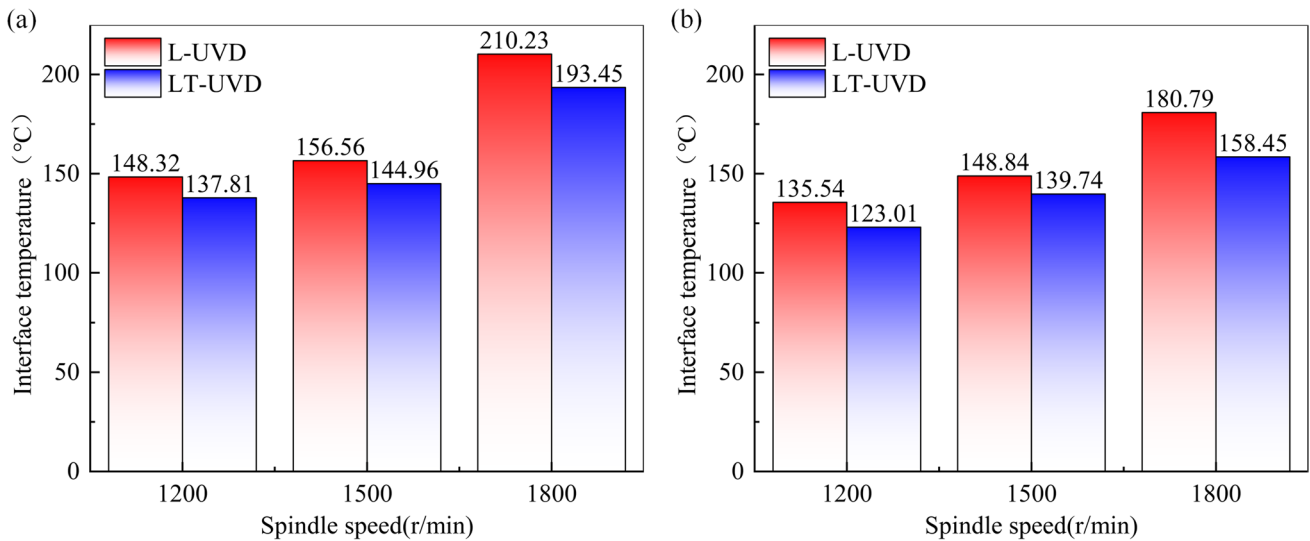

Fig. 12 Variation curves of maximum interface temperature with the rotating speed of the main shaft using different drilling modes (L-UVD and LT-UVD) and different drilling sequences: **a** C to T and **b** T to C

hole inlet and outlet morphology are important foundations for evaluating hole quality. In this section, the dimensional precision of the hole was observed by the GLOBAL S 12.Y.Y.10 three-coordinate measuring system. The morphology of the hole inlet and outlet was observed by the Navitar microscopic observation system. Lastly, the surface roughness and micro-morphology of the observation hole were observed by the KEYENCE VK-X100 laser scanning microscope.

4.3.1 Diameter precision and roundness

The diameter precision and roundness of the hole are important factors that seriously restrict the operation performance in the assembly connection of CFRP/Ti [27]. Each hole was measured several times with the three-coordinate measuring machine to detect the changes in hole sizes using different processing methods, as shown in

Fig. 13. Using LT-UVD, both the hole diameter and roundness of CFRP/Ti were closer to the ideal values and showed remarkable improvement compared to the workpieces processed via CD and L-UVD. This can be explained as follows. LT-UVD can reduce the drilling thrust, lower the drilling temperature, and improve the stability when drilling laminated materials. Accordingly, the interaction between the cutter and the workpiece can be improved, accompanied by a more precise hole size. Even though a set of L-UVD is shown in Fig. 13 with a better hole size for Ti, the error bars using LT-UVD were shorter and characterized by improved roundness. This suggests a more stable drilling process consistent with the above conclusions.

In addition, the hole diameters of CFRP with different drilling sequences are compared in Fig. 13. Drilling from T to C produced the drilling hole of CFRP with better precision. Similar rules can be observed using different drilling modes. For the CFRP on the upper part, the chips produced during Ti drilling on the lower part can corrode the wall of the processed holes of the upper CFRP. Consequently, secondary damages to the CFRP hole wall can occur, and the hole diameter can be enlarged. When the CFRP plate is underneath, the hole size is maintained at the level after processing with higher precision.

4.3.2 Hole wall roughness

In this study, the surface roughness of the hole was examined by the 3D surface morphology under a laser microscope, as shown in Fig. 14a. The measurements were taken multiple times and averaged to lower the interference from external factors. Then, histograms and error bars were plotted,

as shown in Fig. 14b. The hole wall roughness of CFRP and Ti was separately measured, and the roughness was characterized by the Ra value commonly used in CFRP/Ti drilling. According to Fig. 14b, the roughness of CFRP using LT-UVD was 19.80–22.38% and 11.61–12.32% lower than the values using CD and L-UVD, while the roughness of Ti using LT-UVD was reduced by 37.00–62.92% and 14.02–26.91%, respectively. This is because LT-UVD showed better material removal performance and produced a smoother wall of the processed hole. Moreover, the roughness of CFRP when drilling from C to T was generally higher than the value from T to C, which is consistent with the above observation regarding dimensional precision.

4.3.3 Morphologies of the inlet and the outlet of CFRP holes

The morphological images of both inlet and outlet of the CFRP hole using different processing methods (CD, L-UVD, and LT-UVD) were observed using an optical microscope, as shown in Fig. 15. As described in Section 3.2, CRFP is made up of a fibrous woven layer on the one side and an anti-electromagnetic wave metal fiber layer on the other side. Due to different materials on the upper and lower surfaces, the materials corresponding to the outlet and inlet were also different under the two drilling sequences and then separated for analysis.

According to Fig. 15, in contrast with the condition using CD, the delamination defects using L-UVD and LT-UVD at the inlet of CFRP can be significantly suppressed for the T to C sequence. As the cutter drilled out, metal fibers at the CFRP outlet could not be effectively excised, and many
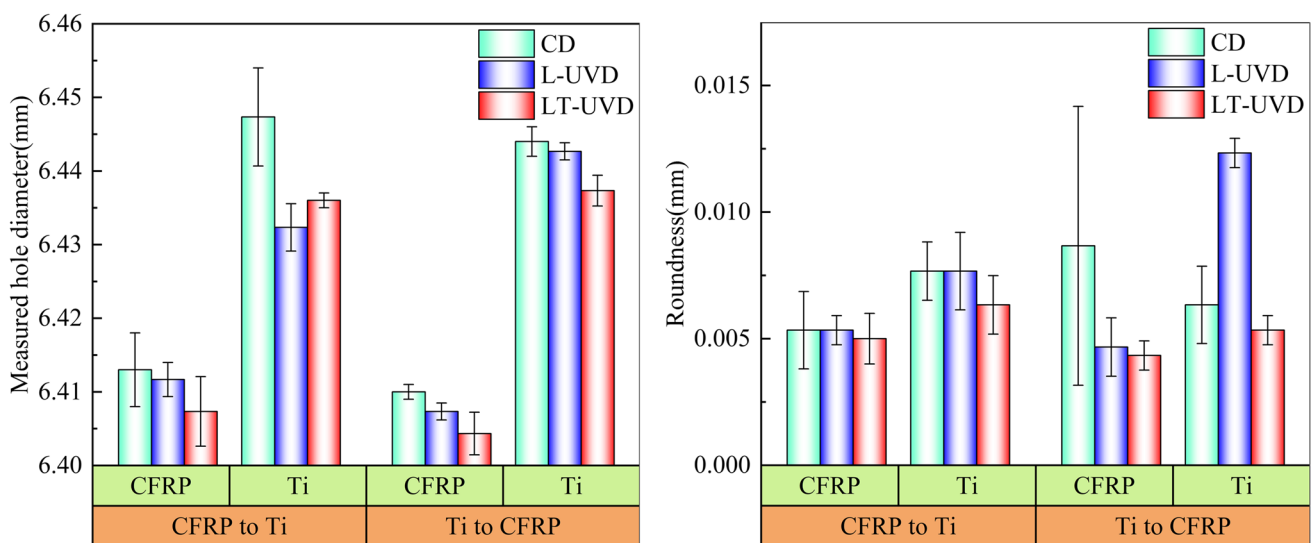

Fig. 13 Comparison of hole diameter accuracy and roundness in CD, L-UVD, and LT-UVD for the same drilling parameters ($n = 10$ mm/min and $V_f = 1200$ r/min)
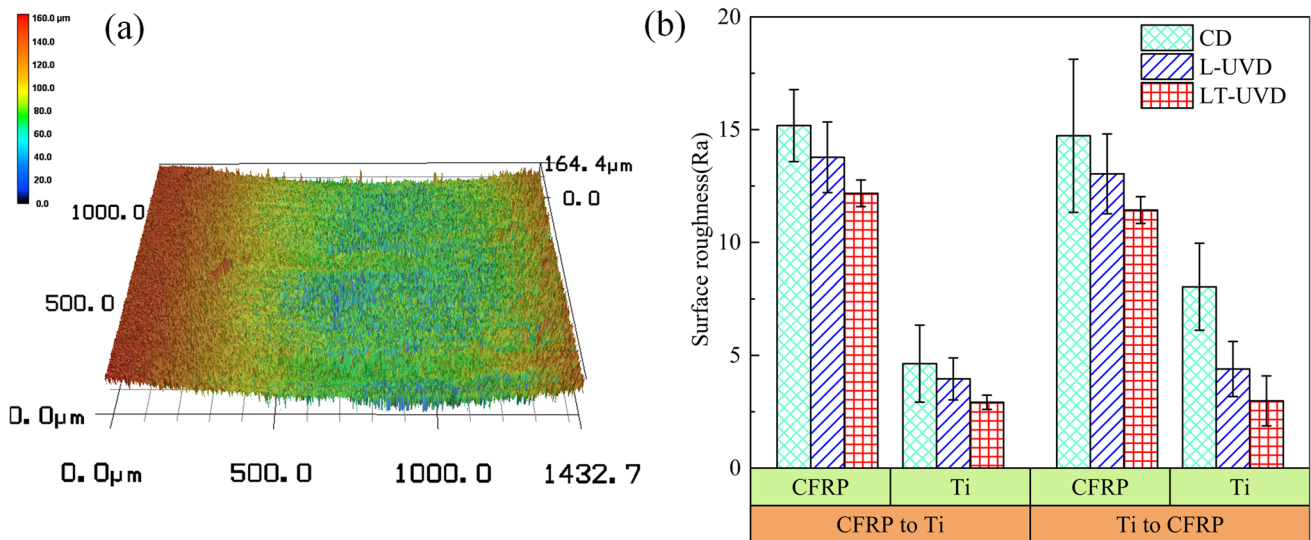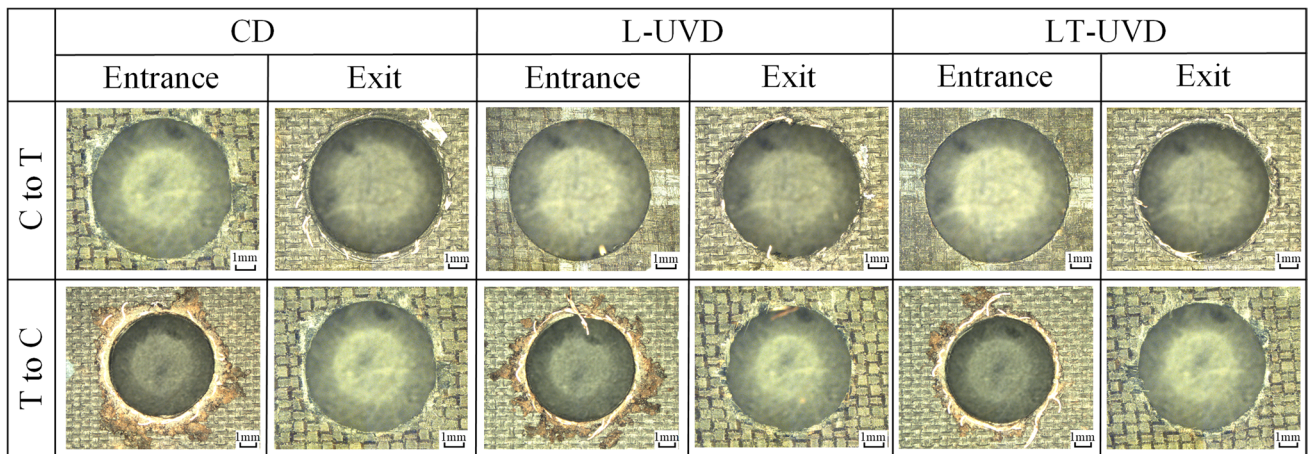
Fig. 14 Comparison of hole diameter accuracy and roundness in CD, L-UVD, and LT-UVD for the same drilling parameters ($n = 10$ mm/min and $V_f = 1200$ r/min)

Fig. 15 Comparison of hole edge morphology of CFRP in CD, L-UVD, and LT-UVD for the same drilling parameters ($n = 10$ mm/min and $V_f = 1200$ r/min)

burrs appeared with the rotation of the cutter. In addition, the metal fiber pullout phenomenon can be effectively suppressed by employing LT-UVD with better fiber-cutting performance. When drilling from T to C, the CFRP chip invasion interface layer was observed at the inlet in addition to the defects of metal fiber pullout. The powder CFRP chips entered the interface layer with the rising of the chip groove on the drilling bit and bonded at the CFRP inlet under high temperature and high pressure at the interface. It can also be observed that CFRP chips were slightly bonded using LT-UVD, with more favorable chip removal performance.

During CFRP/Ti drilling, the delamination of composite materials is always the main cause of material damage. The delamination factor F_d is introduced to characterize the area proportion of the delamination region and quantitatively analyze the delamination defects in CFRP processing. Factor F_d is defined as the ratio of the maximum delamination diameter (D_{max}) to the nominal diameter (D_{nom}), as shown in Fig. 16. The delamination factor F_d when LT-UVD is used dropped by 1.24–6.54% compared to L-UVD. This can be attributed to the direct relation between delamination defects at the CFRP outlet and thrust force. As the drilling continued, the support force brought about the uncut region decreased, and the material was deformed and humped outwards due to an overly large thrust force, leading to the delamination at the hole edge. Additionally, F_d dropped slightly with the increase in the rotating speed. This is consistent with thrust force variation rules.
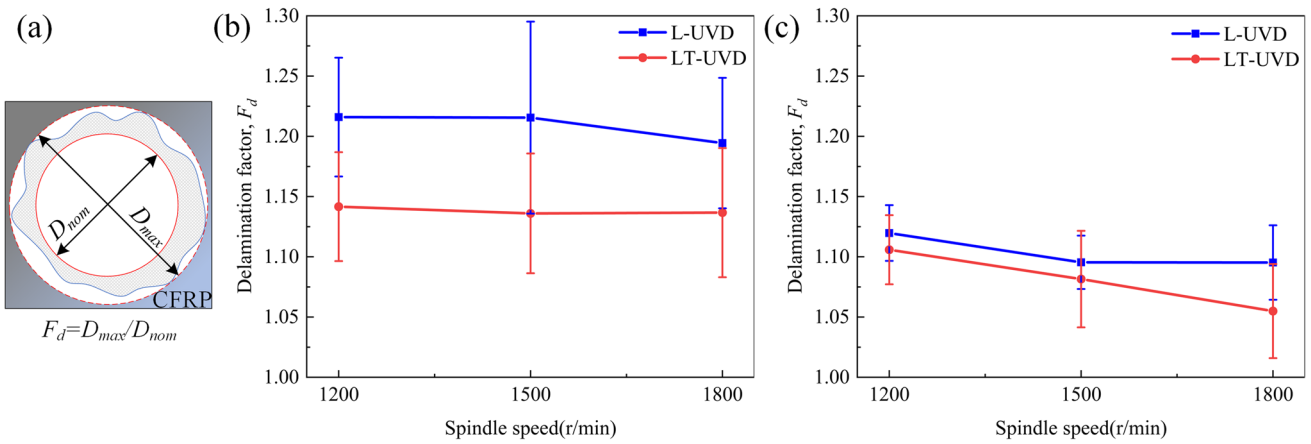
Fig. 16 Comparison of the delamination factor F_d in L-UVD and LT-UVD at different rotating speeds of the main shaft: **a** the illustration of the delamination factor F_d, **b** drilling from C to T, and **c** drilling from T to C

4.3.4 Micro-morphology of the hole wall

Figure 17 displays SEM and laser microscope height images of CFRP hole walls using different drilling methods (CD, L-UVD, and LT-UVD). Cavities, resin scratches, and large-scale continuous fiber pullout can be observed in the CFRP hole of CD, deteriorating the hole wall quality. Compared with CD, ultrasonic vibration drilling can remarkably improve the quality of the hole wall. When L-UVD and LT-UVD were used, no strip scratch defects appeared on the hole wall, and fiber pullout can be lowered in both degree and scale. Combined with the laser microscope height images and profile curves, the profile was still rugged on the hole wall processed with L-UVD. Moreover, a few cavities that seriously affect the hole wall quality can be observed. Using LT-UVD, the processed hole wall was smoother than
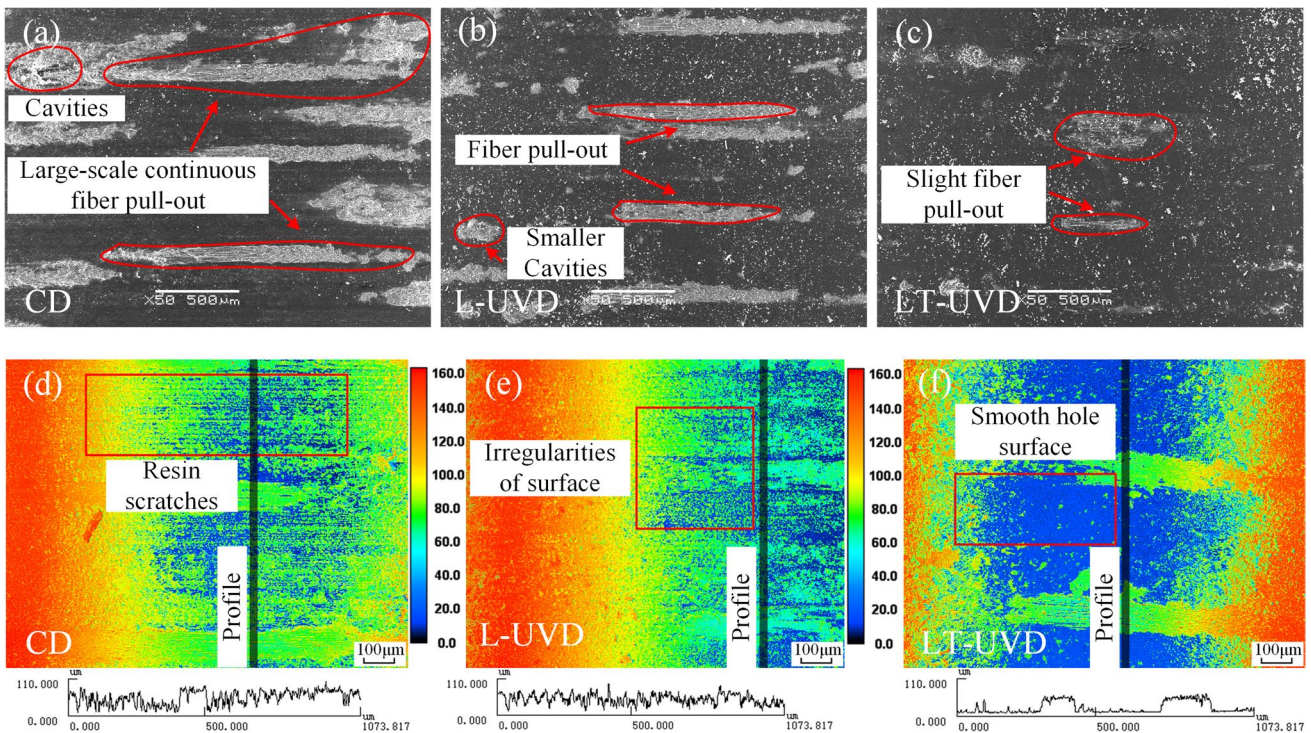

Fig. 17 Comparison of the SEM (**a**–**c**) and laser microscope height (**d**–**f**) images of CFRP holes in CD, L-UVD, and LT-UVD for the same drilling parameters ($n = 10$ mm/min and $V_f = 1200$ r/min)

the condition using L-UVD, and the fiber pullout degree was significantly reduced. The above discussed significant difference in CFRP hole micro-structures among different processing methods can be attributed to unique circumferential vibration in LT-UVD, making carbon fibers prone to fracture and producing smoother fractures.

4.4 High-speed camera experiment

The workpiece edge was drilled by the cutter to observe the interfacial changes during LT-UVD. The exposed cutter and the interface layer in drilling were then recorded by the high-speed camera, as shown in Fig. 18. As shown in Fig. 18(a1), the actual hole wall of CFRP has a large deviation from the hole axis, and the closer to the interface layer, the greater the offset distance. However, the actual hole wall of Ti is close to the hole axis. This shows that in the drilling sequence from C to T, when the tool reached the interface layer, passed through the CRFP and began to drill harder Ti, a rapid increase of thrust force led to the decline in drilling stability. Accordingly, the cutter deviated, which can account for the deflection of the hole wall. This shows that the problems caused by the difference in processing performance between CFRP and Ti have a greater impact on the hole wall quality of CFRP drilling. In addition, as shown in Fig. 18(a2), Ti chips can generate

certain corrosion and damage to the interface during the drilling of the interface layer.

By contrast, no serious deviation appeared along the cutter feeding direction when drilling from T to C, as shown in Fig. 18(b1). However, drilling from T to C also brought about the following problem. An overly high thrust force during Ti drilling led to crushing defects at the interface layer of CFRP. In combination with the observation in Fig. 18(b2), it can also be concluded that the burrs of Ti and chips during the drilling of the interface layer were extruded downwards, thereby causing damage to the lower supporting CFRP plates. The experiment revealed the damage mode at the CFRP/Ti interface, which can provide a reference for high-precision hole preparation.

4.5 Morphology of chips and wear of the cutter

Figure 19 shows the produced Ti chips and the drilling cutters during CFRP/Ti processing using three different drilling modes. Wide and seriously deformed serrated chips were formed during CD drilling. These chips can easily jam the groove and bring about secondary damage to the processed hole wall. Moreover, the cutter was severely worn, while broken and built-up edges appeared. Using L-UVD, chips were narrower and subjected to minor extrusion,
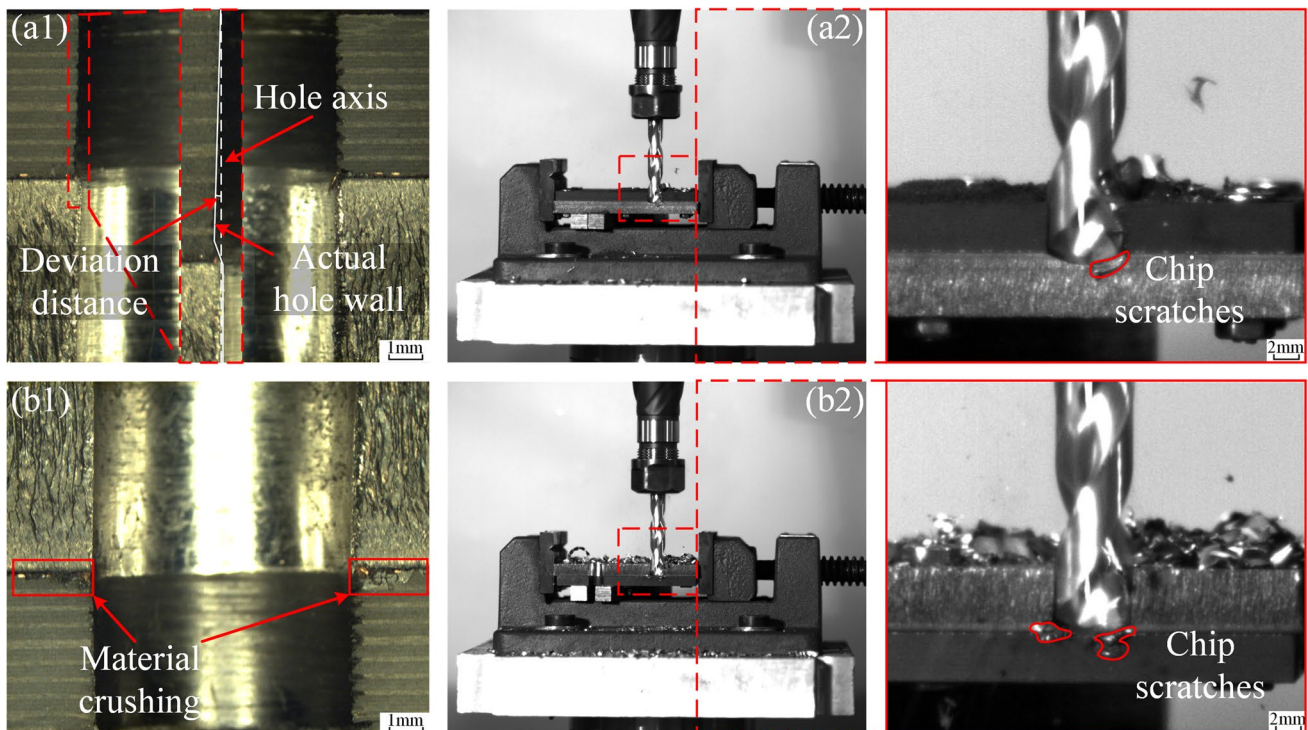

Fig. 18 Observation results using LT-UVD ($n = 10$ mm/min and $V_f = 1200$ r/min) under a high-speed camera: (**a1**) C to T, (**a2**) C to T, (**b1**) T to C, and (**b2**) T to C
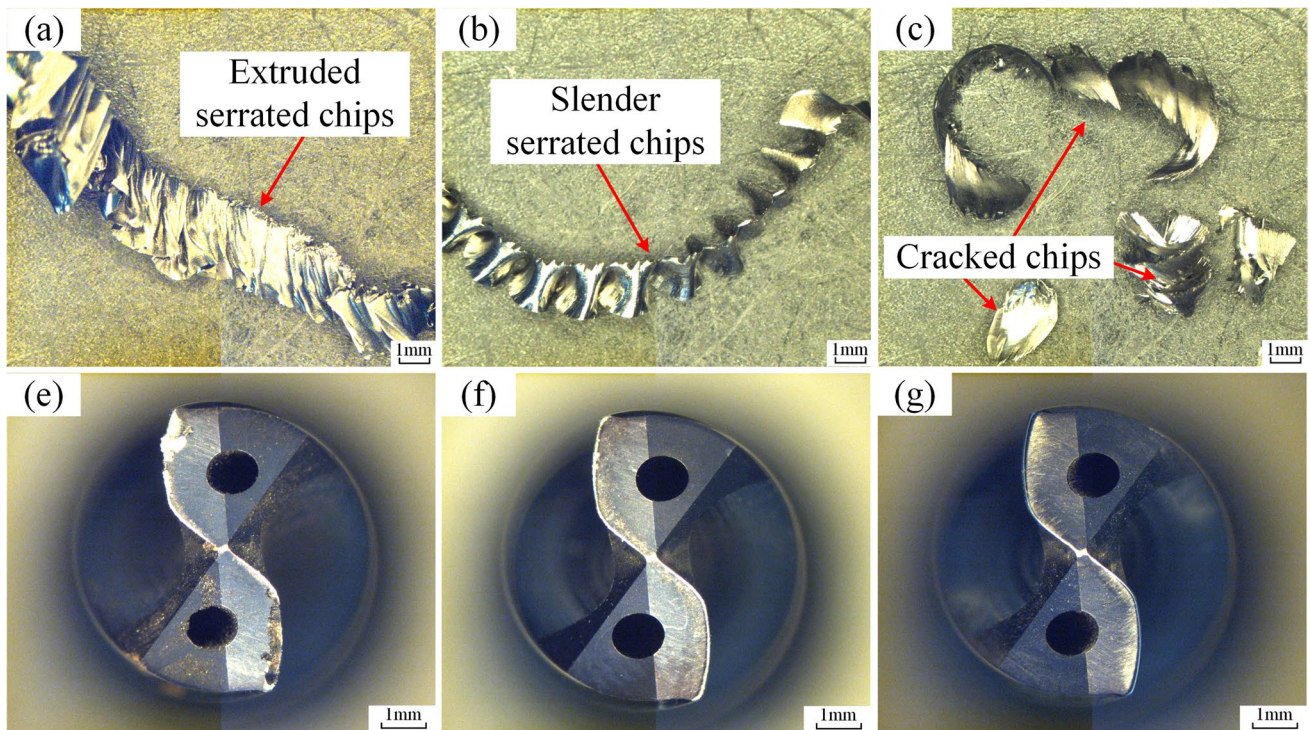
Fig. 19 Morphological patterns of chips and cutter wear conditions using different drilling modes and the same drilling parameters ($n = 10$ mm/min and $V_f = 1200$ r/min): **a** CD, **b** L-UVD, **c** LT-UVD, **e** CD, **f** L-UVD, and **g** LT-UVD

significantly improving the chip removal performance and cutter wear.

It should be noted that Ti chips in LT-UVD were different from CD and L-UVD. When LT-UVD was employed, the produced chips were crushed under longitudinal-torsional vibration, thereby forming finer chips. Accordingly, both chip-breaking performance and surface integrity can be further improved. The cutter using LT-UVD was more slightly worn than the cutters using the other two drilling modes, with a more complete main cutting edge.

5 Conclusions

In this paper, experimental drilling studies of CFRP/Ti stacks were conducted for CD, L-UVD, and LT-UVD processes. Based on the innovative LT-UVD vibration actuator, drilling experiments with different drilling methods and processing parameters were conducted to evaluate the quality of LT-UVD without cutting fluid in many aspects. Finally, the experimental results showed that LT-UVD could effectively improve the drilling quality of CFRP/Ti stacks from the perspectives of thrust force, interface temperature, hole wall quality, and drilling defects. The following conclusions can be drawn:

1. Under the same processing parameters, the thrust force in L-UVD and LT-UVD significantly decreased relative to CD (16.27–40.55% in CFRP and 17.37–24.83% in Ti). In addition, further comparison between L-UVD and LT-UVD demonstrated that the thrust force of CFRP in LT-UVD decreases by 2.04–14.61%, while the thrust force of Ti decreases by 1.95–9.34%. This can be attributed to unique torsional vibration in LT-UVD, which has a better material removal effect.

2. The temperature of the interface layer in CD is increased (up to 214.88 °C), while the interface temperature of L-UVD and LT-UVD decreased by roughly 30–40% relative to the CD. Furthermore, due to the chip-breaking performance and thrust force improvement during processing, the interface temperature of LT-UVD was further reduced by approximately 6–12%, compared with L-UVD.

3. Due to a decrease in thrust force and interface temperature in LT-UVD, the hole diameter accuracy and roundness were greatly improved. Moreover, the delamination factor F_d of CFRP was reduced by 1.24–6.54% compared to L-UVD. Compared with CD and L-UVD, CFRP and Ti surface roughness were improved (i.e., a maximum decrease of 22.38% and 62.92%, respectively) due to torsional vibrations in LT-UVD that contributed to fiber breakage and metal material removal.

4. CD, L-UVD, and LT-UVD were all characterized by mechanical damage. However, an inspection of the micro-morphology of the CFRP hole wall found that the hole wall of LT-UVD was smoother, no stripe scratch defects were observed, and the cavity and fiber pullout defects were greatly reduced.

5. The experiments filmed by the high-speed camera show that the drilling stability at the interface was reduced due to different processing properties between the two materials in CFRP/Ti drilling, such as the hole wall deflection problem in the C to T drilling sequence and brittle CFRP crushing defect in the T to C sequence.

6. Long serrated chips often appear in CD and L-UVD, which can easily cause clogging of the chip groove and increase tool wear. In LT-UVD, the chips were broken during drilling due to longitudinal-torsional vibration. Hence, chip-breaking performance was improved, and the tool wear was reduced.

Declarations

References

1. Wang B, Wang Y, Zhao H, Lei S, Wang M, Kong X (2020) Effect of a Ti alloy layer on CFRP hole quality during helical milling of CFRP/Ti laminate. Compos struct 252:112670. https://doi.org/10.1016/j.compstruct.2020.112670

2. Kumar D, Gururaja S, Jawahir IS (2020) Machinability and surface integrity of adhesively bonded Ti/CFRP/Ti hybrid composite laminates under dry and cryogenic conditions. J Manuf Process 58:1075–1087. https://doi.org/10.1016/j.jmapro.2020.08.064

3. Jia Z, Zhang C, Wang F, Fu R, Chen C (2019) An investigation of the effects of step drill geometry on drilling induced delamination and burr of Ti/CFRP stacks. Compos struct 235:111786. https://doi.org/10.1016/j.compstruct.2019.111786

4. Wang Q, Wang F, Zhang C, Chen C (2020) Combined effects of various materials on tool wear in drilling of Ti/CFRP stacks. P I Mech Eng C-J Mec 234(14):2750–2759. https://doi.org/10.1177/0954406219868246

5. Suo H, Wei Z, Zhang K, Deng K, Cheng H, Luo B, Li H, Wang L, Liang B (2022) Interfacial wear damage of CFRP/Ti-alloy single-lap bolted joint after long-term seawater aging. Eng Fail Anal 139:106464. https://doi.org/10.1016/j.engfailanal.2022.106464

6. Kolesnyk V, Peterka J, Alekseev O, Neshta A, Xu J, Lysenko B, Sahul M, Martinovič J, Hrbal J (2022) Application of ANN for analysis of hole accuracy and drilling temperature when drilling CFRP/Ti alloy stacks. Materials 15(5):1940. https://doi.org/10.3390/ma15051940

7. Zhang Z, Zhang N, Wu F, Teng W, Sun Y, Guo B (2022) Research on variable parameter drilling method of Ti-CFRP-Ti laminated stacks based on real-time sensing of drilling axial force. Sensors 22(3):1188. https://doi.org/10.3390/s22031188

8. An Q, Zhong B, Wang X, Zhang H, Sun X, Chen M (2021) Effects of drilling strategies for CFRP/Ti stacks on static mechanical property and fatigue behavior of open-hole CFRP laminates. J Manuf Process 64:409–420. https://doi.org/10.1016/j.jmapro.2021.01.036

9. Fernández-Pérez J, Cantero JL, Díaz-Álvarez J, Miguélez MH (2017) Influence of cutting parameters on tool wear and hole quality in composite aerospace components drilling. Compos struct 178:157–161. https://doi.org/10.1016/j.compstruct.2017.06.043

10. Luo B, Zhang K, Liu S, Cheng H, Wang R (2019) Investigation on the interface damage in drilling low-stiffness CFRP/Ti stacks. Chinese J Aeronaut 32(9):2211–2221. https://doi.org/10.1016/j.cja.2019.04.017

11. Samsudeensadham S, Krishnaraj V (2022) Drilling study on CFRP/Ti-6Al-4V stacks using chip breaker grooved drill. Mater Manuf Process 37(13):1511–1525. https://doi.org/10.1080/10426914.2022.2030872

12. Jia Z, Zhang C, Wang F, Fu R, Chen C (2020) Multi-margin drill structure for improving hole quality and dimensional consistency in drilling Ti/CFRP stacks. J Mater Process Tech 276:116405. https://doi.org/10.1016/j.jmatprotec.2019.116405

13. Alonso U, Calamaz M, Girot F, Iriondo E (2019) Influence of flute number and stepped bit geometry when drilling CFRP/Ti6Al4V stacks. J Manuf Process 39:356–370. https://doi.org/10.1016/j.jmapro.2019.02.006

14. Qiu X, Yu Z, Li C, Niu Q, Li S, Li P, Ko TJ (2021) Influence of main cutting edge structure on hole defects in CFRP/titanium alloy stacks drilling. J Manuf Process 69:503–513. https://doi.org/10.1016/j.jmapro.2021.07.061

15. Shao Z, Jiang X, Li Z, Geng D, Li S, Zhang D (2019) Feasibility study on ultrasonic-assisted drilling of CFRP/Ti stacks by single-shot under dry condition. Int J Adv Manuf Tech 105(1–4):1259–1273. https://doi.org/10.1007/s00170-019-04329-2

16. Shao Z, Jiang X, Geng D, Liu Y, Zhou Z, Li S, Zhang D, Zheng W (2021) The interface temperature and its influence on surface integrity in ultrasonic-assisted drilling of CFRP/Ti stacks. Compos struct 226:113803. https://doi.org/10.1016/j.compstruct.2021.113803

17. Dahnel AN, Barnes S, Ascroft H, Gloger M (2015) Analysis of tool wear and hole quality during ultrasonic assisted drilling (UAD) of carbon fibre composite (CFC)/titanium alloy (Ti6Al4V)

stacks. ASME Int Mech Eng Congress Expo. https://doi.org/10.1115/IMECE2015-50416.IMECE2015-50416

18. Liu Y, Li Q, Qi Z, Chen W (2021) Defect suppression mechanism and experimental study on longitudinal torsional coupled rotary ultrasonic assisted drilling of CFRPs. J Manuf Process 70:177–192. https://doi.org/10.1016/j.jmapro.2021.08.042

19. Ma G, Kang R, Dong Z, Yin S, Bao Y, Guo D (2020) Hole quality in longitudinal–torsional coupled ultrasonic vibration assisted drilling of carbon fiber reinforced plastics. Front Mech Eng-Prc 15:(538–546). https://doi.org/10.1007/s11465-020-0598-y

20. Wang X, Jiao F, Wang D, Niu Y (2019) Development of a longitudinal–torsional ultrasonic vibration-aided drilling system for drilling carbon fiber-reinforced polymer materials. P I Mech Eng C-J Mec 233(12):4176–4186. https://doi.org/10.1177/0954406219833084

21. Liu Y, Pan Z, Li Q, Qi Z, Chen W (2022) Experimental and scale-span numerical investigations in conventional and longitudinal torsional coupled rotary ultrasonic–assisted drilling of CFRPs. Int J Adv Manuf Tech 199(3–4):1707–1724. https://doi.org/10.1007/s00170-021-08286-7

22. Tian Y, Zou P, Kang D, Fan F (2021) Study on tool wear in longitudinal-torsional composite ultrasonic vibration–assisted drilling of Ti-6Al-4V alloy. Int J Adv Manuf Tech 113(7–8):1989–2002. https://doi.org/10.1007/s00170-021-06759-3

23. Gao G, Xia Z, Yuan Z, Xiang D, Zhao B (2021) Influence of longitudinal-torsional ultrasonic-assisted vibration on micro-hole drilling Ti-6Al-4V. Chinese J Aeronaut 34(9):247–260. https://doi.org/10.1016/j.cja.2020.06.012

24. Xu J, Ji M, Paulo Davim J, Chen M, El Mansori M, Krishnaraje V (2020) Comparative study of minimum quantity lubrication and dry drilling of CFRP/titanium stacks using TiAlN and diamond coated drills. Compos Struct 234:111727. https://doi.org/10.1016/j.compstruct.2019.111727

25. An Q, Dang J, Li J, Wang C, Chen M (2020) Investigation on the cutting responses of CFRP/Ti stacks: With special emphasis on the effects of drilling sequences. Compos Struct 253:112794. https://doi.org/10.1016/j.compstruct.2020.112794

26. Xu J, El Mansori M (2016) Experimental study on drilling mechanisms and strategies of hybrid CFRP/Ti stacks. Compos Struct 157:461–482. https://doi.org/10.1016/j.compstruct.2016.07.025

27. Geng D, Zhang D, Li Z, Liu D (2017) Feasibility study of ultrasonic elliptical vibration-assisted reaming of carbon fiber reinforced plastics/titanium alloy stacks. Ultrasonics 75:80–90. https://doi.org/10.1016/j.ultras.2016.11.011